PNAS PLUS

Classification of topological phonons in linear mechanical metamaterials

Roman Süsstrunk[a,1] and Sebastian D. Huber[a]

[a]Institute for Theoretical Physics, ETH Zürich, 8093 Zurich, Switzerland

Edited by Mordechai (Moti) Segev, Technion–Israel Institute of Technology, Haifa, Israel, and approved June 21, 2016 (received for review April 4, 2016)

Topological phononic crystals, alike their electronic counterparts, are characterized by a bulk–edge correspondence where the interior of a material dictates the existence of stable surface or boundary modes. In the mechanical setup, such surface modes can be used for various applications such as wave guiding, vibration isolation, or the design of static properties such as stable floppy modes where parts of a system move freely. Here, we provide a classification scheme of topological phonons based on local symmetries. We import and adapt the classification of noninteracting electron systems and embed it into the mechanical setup. Moreover, we provide an extensive set of examples that illustrate our scheme and can be used to generate models in unexplored symmetry classes. Our work unifies the vast recent literature on topological phonons and paves the way to future applications of topological surface modes in mechanical metamaterials.

topological matter | mechanical metamaterials | adaptive materials

Mechanical metamaterials derive their properties not from their microscopic composition but rather through a clever engineering of their structure at larger scales (1). Various design principles have been put forward and successfully applied in the past. Examples range from periodic modifications leading to band gaps via Bragg scattering (2) to the use of local resonances (3) to achieve subwavelength functionalities. Recently, the concept of "band topology" emerged as a new design principle for mechanical metamaterials (4–14). Colloquially speaking, a system with a topological phonon band structure will possess mechanical modes bound to surfaces or lattice defects that are immune to a large class of perturbations. If the targeted purpose of a metamaterial is encoded in such a topologically protected mode, its functioning will be largely independent of production imperfections or environmental influences.

The introduction of topology to the field of mechanical metamaterials was largely motivated by its successful application to the description of electrons in solids (15) and to photonics (16–19). One of the key elements in the understanding of the electronic systems was the classification of different topological phases according to their symmetry properties (20–22). Although over the last years numerous proposals (4, 5, 23–42) and several experiments (6–14) were put forward promoting mechanical topological metamaterials, a complete classification of linear topological phonons is missing to date. In this report, we intend to fill in this gap.

At first sight, the dynamics in classical mechanics seems to be rather different from quantum-mechanical electron systems. Our approach is therefore to map the first to the second problem (26). This, in principle, allows us to import the classification (20, 21) from the description of electronic systems. However, a bare import of this classification is not doing justice to the rich structure mechanical systems possess by themselves.

We can categorize mechanical metamaterials by two independent properties. First, the targeted functionality can either be at zero or at finite frequencies. Zero-frequency modes define structural properties such as mechanisms where parts of a material move freely (5, 8). The dual partners of freely moving parts are states of self-stress (35), where external loads on a material can be absorbed in the region of a topological boundary mode. Defining such details of the load-bearing properties of a material are relevant both for smart adaptive materials (9) as well as for civil engineering applications. The design of finite-frequency properties, on the other hand, constitutes a quite different field of research. Here, the goals are to control the propagation, reflection, or absorption of mechanical vibrations. This includes, for example, waveguiding, acoustic cloaking, or vibration isolation ranging from the seismic all of the way to the radiofrequency scale.

A second important separation into two distinct classes of materials arises from the presence or absence of nonreciprocal elements (43). Generically, nondissipative mechanical properties are invariant under the reversal of the arrow of time. Nonreciprocal elements, however, transmit waves asymmetrically between different points in space. The absence of time-reversal symmetry allows for a topological invariant, the Chern number, which encodes chiral, or unidirectional wave propagation. We will see that these two attributes: static vs. dynamic and reciprocal vs. nonreciprocal will be key to understand how the electronic classification is naturally modified for mechanical systems.

Before we embark on the development of the framework needed for our classification, let us state our goals more precisely. Our aim is to import and adapt the classification of noninteracting electron systems according to their local symmetries $\mathcal{T}$, $\mathcal{C}$, and $\mathcal{S}=\mathcal{T}\circ\mathcal{C}$, that is, time reversal, charge conjugation, and their combination, respectively (20, 21). Clearly, we will have to specify the role of these symmetries in mechanical systems. Moreover, we cover only the "strong" indices, which do not rely on any spatial symmetries. The extension to weak indices, arising from a stacking of lower-dimensional systems carrying strong indices, is straightforward (5). Finally, there are many recent developments dealing with topological phases stabilized by spatial

Significance

A mechanical metamaterial is an engineered material that is characterized by properties that go beyond the properties of its microscopic building blocks. Specifically, in topological metamaterials, one makes use of surface or boundary modes that are stable against imperfections or environmental influences and hence constitute reliable building blocks for various applications. In our work, we provide a classification scheme of possible topological metamaterials and an extensive number of examples illustrating this scheme. Our classification can serve as an important blueprint for many future applications that target such stable boundary modes for engineering purposes.

Author contributions: R.S. and S.D.H. designed research, performed research, and wrote the paper.

The authors declare no conflict of interest.

This article is a PNAS Direct Submission.

[1]To whom correspondence should be addressed. Email: suesstrunk@itp.phys.ethz.ch.

This article contains supporting information online at www.pnas.org/lookup/suppl/doi:10.1073/pnas.1605462113/-/DCSupplemental.

properties (44–48) such as point group symmetries. Although such spatial symmetries are more easily broken by disorder, the required ingredients might be very well tailored to the mechanical setup (49, 50).

The remainder of this paper is organized as follows: we start by developing a framework to map classical problems to an equation that formally looks like a Schrödinger equation of a quantum-mechanical problem. We then introduce the three symmetries, $\mathcal{T}$, $\mathcal{C}$, and $\mathcal{S}$, and discuss their appearance in mechanical problems before we provide the sought classification. Finally, an extensive example section serves two purposes: we illustrate and apply our approach. Moreover, we show a way how to construct new symmetry classes from generic building blocks.

Models and Theoretical Framework

In this manuscript, we aim at characterizing discrete systems of undamped, linear mechanical oscillators. Although this setup is directly relevant for simple mass-spring systems (11) or magnetically coupled gyroscopes (12), the scope here is actually considerably broader. Any system that can be reliably reduced to a discrete linear model is amenable to our treatment. This includes 1D (40), 2D (25, 38, 39, 41), or 3D (40) systems made from continuous media, where a targeted microstructuring enables the description in terms of a discrete model. Once we deal with a discrete model, we have a direct way to import the methods known from electronic topological insulators. To establish this bridge, we now introduce a formal mapping of a classical system of coupled oscillators to a tight-binding hopping problem of electrons in solids.

We start with the equations of motion of a generalized mass-spring model given by

$$\ddot{x}_i(t) = \sum_{j=1}^{N} \left[-D_{ij} x_j(t) + \Gamma_{ij} \dot{x}_j(t) \right]. \qquad [1]$$

Here, t denotes time; $x_i(t) \in \mathbb{R}$, one of the N independent displacements; and $\dot{x}_i(t)$, its time derivative. The mass terms are absorbed into the real and constant coupling elements D_{ij} and Γ_{ij}. The entries D_{ij} can be thought of as springs coupling different degrees of freedom, and Γ_{ij} arise from velocity-dependent forces. Note, that a nonzero Γ implies terms formally equivalent to the Lorentz force of charged particles in a magnetic field and hence arise only in metamaterials with nonreciprocal elements. In addition to constant coupling elements in 1, one can also consider periodically driven systems. Such driven system can be cast into our framework by a suitable (Magnus) expansion of the corresponding Floquet operator (37, 51, 52).

We aim at rewriting Eq. **1** in the form of a Schrödinger equation, or rather as a Hermitian eigenvalue problem. Therefore, we need the system to be conservative (nondissipative). This is achieved by requiring D to be symmetric positive-definite and Γ to be skew-symmetric.[‡]

An eigenvalue problem emerges from Eq. **1** via the ansatz $x_i(t) = e^{-i\lambda t} x_i(0)$:

$$\lambda \vec{y} = i \begin{pmatrix} 0 & 1 \\ -D & \Gamma \end{pmatrix} \vec{y}, \qquad \vec{y} = \begin{pmatrix} \vec{x}(0) \\ \dot{\vec{x}}(0) \end{pmatrix}, \qquad [2]$$

where we gathered the indices i in a vector notation $\vec{x}(t)$. Energy conservation requires all eigenvalues λ to be real, but the ansatz renders the problem complex. However, a suitable superposition of complex eigensolutions always allows to create real solutions with $\vec{x}(t) \in \mathbb{R}^N$.

Although Eq. **2** contains all of the information about the eigensolutions, for the topological classification it is advantageous to transform it into a Hermitian form. To this end, we apply the transformation

$$T = \begin{pmatrix} \sqrt{D} & 0 \\ 0 & i \end{pmatrix} \qquad [3]$$

to $\vec{y}$. The square root of the matrix D is defined through its spectral decomposition, where the positive branch of the square root of the eigenvalues is chosen. With this, we arrive at

$$i \frac{d}{dt} \vec{\psi}(t) = H \vec{\psi}(t), \quad \vec{\psi}(t) = e^{-i\lambda t} T \vec{y}, \quad H = \begin{pmatrix} 0 & \sqrt{D} \\ \sqrt{D} & i\Gamma \end{pmatrix}. \qquad [4]$$

As D is symmetric positive-definite and Γ is skew-symmetric, the matrix H is Hermitian and the differential equation for $\vec{\psi}$ has the sought-after form of a Schrödinger equation.

The formulation in Eq. **4** is reminiscent of a single-particle tight-binding problem in quantum mechanics. Therefore, the discussion of topological properties of the eigenvectors $\vec{\psi}$ can be directly carried over. Remember that the topological classification is based on the spatial dimensionality of the problem as well as properties of special local symmetries alone. In particular, the topological properties do not rely on translational symmetries. However, their discussion and definitions are most conveniently introduced for translationally symmetric systems. In this case, the D and Γ matrices are periodic and a spatial Fourier transform block-diagonalizes them (one block for each wave vector $\vec{k}$). It follows that $\sqrt{D}$ becomes block diagonal as well, because it shares its eigenvectors with D. Hence, we will discuss families $H(\vec{k})$ of Hamiltonians of the form 4.

Before turning our attention to the topological classification, we comment on two more points: (*i*) the influence of damping and (*ii*) the possibility for alternative Hermitian forms. Every real system is prone to damping, which in turn affects the eigensolutions in two ways. The eigenvalues acquire an imaginary part and the form of the eigenvectors may change. Although a slight change of the eigenvalues does not influence the subsequent discussion, the difference in the eigenvectors may alter the results. Whether or not it obstructs the use or observation of a given topological effect depends on the details of the specific system.

Now to the second point. The transformation leading to Eq. **4** is not the only way to introduce a Hermitian problem. In fact, any decomposition of the form $D = QQ^T$, $Q \in \mathbb{R}^{N \times M}$ will allow us to achieve this goal. By introducing the auxiliary variables $\vec{\eta}(t) = Q^T \vec{x}(t)$, we may express Eq. **1** as

$$i \frac{d}{dt} \begin{pmatrix} \vec{\eta}(t) \\ i\dot{\vec{x}}(t) \end{pmatrix} = \begin{pmatrix} 0 & Q^T \\ Q & i\Gamma \end{pmatrix} \begin{pmatrix} \vec{\eta}(t) \\ i\dot{\vec{x}}(t) \end{pmatrix}. \qquad [5]$$

The particular choice $Q = \sqrt{D} = Q^T$ has the advantage that (*i*) $\sqrt{D}$ has the same eigenvectors as D, (*ii*) it uses only as many auxiliary degrees of freedom as needed, (*iii*) it allows to directly block-diagonalize the problem in absence of Γ, and (*iv*) it offers a canonical way how to choose Q.

Nevertheless, this is not the only useful choice of Q. The starting point for our choice was a given D and Γ, originating from an effective model. In certain cases, however, there is a natural choice of Q along with a physical meaning. Such cases have been considered by Kane and Lubensky (5, 35). In their setup the matrix Q corresponds to the equilibrium matrix of a

[‡]Such matrices can, for example, be obtained from a system with Lagrangian $\mathcal{L} = \sum_{ij} \dot{x}_i A_{ij} \dot{x}_j + x_i B_{ij} \dot{x}_j - x_i C_{ij} x_j$, A_{ij}, B_{ij}, $C_{ij} \in \mathbb{R}$, given that $D = (A + A^T)^{-1}(C + C^T) > 0$.

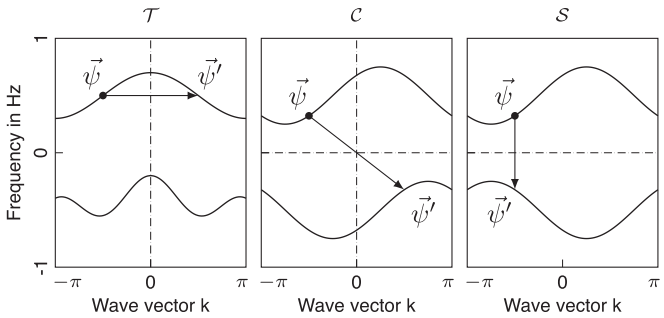

Fig. 1. Visualization of $\mathcal{T}$, $\mathcal{C}$, and $\mathcal{S}$ symmetries by three prototypical band structures. The presence of a symmetry implies a certain symmetry in the band structure (but not the other way around) (see text).

mass-spring model, where Q relates spring tensions to displacements of the attached masses. This allows for a beautiful discussion of (topological) states of self-stress in isostatic lattices (5, 35). Although such states of self-stress elude our description, the formulation of Kane and Lubensky is only applicable to the restricted set of isostatic models, which makes it not the favorite choice for the purpose of our discussion.

Symmetries

As mentioned before, the classification of electronic systems is based on three symmetries: time-reversal symmetry $\mathcal{T}$, particle-hole symmetry $\mathcal{C}$, and chiral symmetry $\mathcal{S}$. In the quantum-mechanical case, these symmetries are represented by (anti)unitary operators on the single-particle Hilbert space. For the present context of classical mechanical systems, it is important to note that these symmetries are merely a set of constraints on the Bloch Hamiltonians $H(\vec{k})$ (21). We state here the form of these constraints and discuss their relation to natural symmetries of mechanical systems below.

We call a system $\mathcal{T}$ symmetric if

$$U_{\mathcal{T}}H\left(\vec{k}\right)-H\left(-\vec{k}\right)U_{\mathcal{T}}=0,\qquad U_{\mathcal{T}}^2=\pm 1, \qquad [6]$$

for some antiunitary $U_{\mathcal{T}}$, which represents $\mathcal{T}$. For the particle-hole symmetry $\mathcal{C}$, the respective criterion is

$$U_{\mathcal{C}}H\left(\vec{k}\right)+H\left(-\vec{k}\right)U_{\mathcal{C}}=0,\qquad U_{\mathcal{C}}^2=\pm 1, \qquad [7]$$

with $U_{\mathcal{C}}$ antiunitary. Finally, the chiral symmetry $\mathcal{S}$, we demand

$$U_{\mathcal{S}}H\left(\vec{k}\right)+H\left(\vec{k}\right)U_{\mathcal{S}}=0,\qquad U_{\mathcal{S}}^2=1, \qquad [8]$$

for a unitary $U_{\mathcal{S}}$ (Fig. 1).

For a generic Hilbert space $\mathcal{H}$, there are no additional restrictions on the representations U, but here the "Hilbert space" has additional structure. Any eigenvector $\vec{\psi}$ is of the form $(\sqrt{D}\vec{x}(0),\lambda\vec{x}(0))$. Hence, after fixing the first half of the entries of $\vec{\psi}$, the remaining half is known as well. It follows that any (anti)unitary mapping $U:\mathcal{H}\to\mathcal{H}$ can be written as

$$U=\begin{pmatrix} W & 0\\ 0 & V\end{pmatrix}, \qquad [9]$$

with V and W (anti)unitary. Let us have a closer look at the three symmetries 6–8 within this framework.

From the definitions, it follows that H has $\mathcal{T}$ symmetry if and only if we can find V, such that

$$V\Gamma\left(\vec{k}\right)+\Gamma\left(-\vec{k}\right)V=0,\qquad VD\left(\vec{k}\right)-D\left(-\vec{k}\right)V=0, \qquad [10]$$

with $W=V$. We refer to it as $\mathcal{T}$ symmetry, instead of "time reversal," because in the setting of classical mechanics it does no longer correspond to the reversal of time. In general, the presence of $\mathcal{T}$ symmetry relies on fine-tuning of parameters, whereas in case that $\Gamma=0$ there is a generic $\mathcal{T}$ symmetry:

$$U_{\mathcal{T}}=\begin{pmatrix}1 & 0\\ 0 & 1\end{pmatrix}\kappa,\qquad U_{\mathcal{T}}^2=1, \qquad [11]$$

where κ is the complex conjugation operator. Note that, even though Γ has the potential to break $\mathcal{T}$ symmetry, $\Gamma\neq 0$ does not imply the absence of it.

For $\mathcal{C}$ symmetry, the conditions to be satisfied are

$$V\Gamma\left(\vec{k}\right)-\Gamma\left(-\vec{k}\right)V=0,\qquad VD\left(\vec{k}\right)-D\left(-\vec{k}\right)V=0, \qquad [12]$$

with $W=-V$. Therefore, for any D and Γ, we can find a particle-hole symmetry

$$U_{\mathcal{C}}=\begin{pmatrix}1 & 0\\ 0 & -1\end{pmatrix}\kappa,\qquad U_{\mathcal{C}}^2=1. \qquad [13]$$

The existence of this omnipresent particle-hole symmetry is nothing but the statement that, for every eigensolution, its complex conjugate is also an eigensolution. Its presence is based on D and Γ being real.

In case we have $\mathcal{T}$ and particle-hole symmetry, we can combine the two to obtain a unitary operator $U_{\mathcal{S}}=U_{\mathcal{C}}U_{\mathcal{T}}$. This unitary operator represents a chiral symmetry. We can therefore conclude that, if $\Gamma=0$, we always have a chiral symmetry

$$U_{\mathcal{S}}=\begin{pmatrix}1 & 0\\ 0 & -1\end{pmatrix}. \qquad [14]$$

This symmetry is nothing but classical time-reversal symmetry, as every eigenvector is mapped to itself and the corresponding eigenvalue becomes minus itself.

So far, particle-hole and chiral symmetries were defined with respect to $\omega=0$, meaning that an eigensolution $(\vec{\psi},\lambda)$ is related to an eigensolution $(\vec{\psi}'=U\vec{\psi},\omega-\lambda)$ with $\omega=0$ (Fig. 1). However, for the purpose of topological indices, we can weaken this requirement. A potentially $\vec{k}$-dependent shift in ω does not change the form of the eigenvectors. Hence, it is sufficient to require the right-hand side of Eqs. **7** and **8** to equal to $2\omega(\vec{k})U_{\mathcal{C}/\mathcal{S}}$ instead of zero. Furthermore, particle-hole and chiral symmetries can also exist only on parts of the band structure, which means that it is possible to have these symmetries on a subspace of all of the solutions only.

These two generalizations of $\mathcal{C}$ and $\mathcal{S}$ symmetries arise naturally in the setting of mass-spring models.[§] Assume that D, which is a real, symmetric matrix and therefore Hermitian, has a particle-hole symmetry with respect to $\omega\neq 0$, and that $\Gamma=0$. Then, all of the eigenvectors of H with positive eigenvalue have a particle-hole symmetry with respect to some $\omega(\vec{k})$, whereas all of the eigenvectors of H with negative eigenvalue have one with respect to $-\omega(\vec{k})$. The matrix $H(\vec{k})$ can be made block-diagonal with the two blocks $\pm\sqrt{D}$ and each corresponding subspace of solutions has a particle-hole (and chiral) symmetry with respect to $\pm\omega(\vec{k})$.

[§]Note that these generalizations are not the only ones possible. However, they emerge naturally in our present discussion.

After discussing the above symmetries, we have all elements we need to establish a topological classification of generic mechanical systems.

Classification

With the mapping of the equations of motion to a Hermitian eigenvalue problem, we can in principle directly use the classification scheme of noninteracting electron systems (20, 21). However, the specific properties of the local symmetries discussed above warrant a more careful discussion. To make further progress, we highlight the most important concepts behind the electronic classification. For a more detailed review, we refer the reader to the excellent recent review by Chiu et al. (53). A reader not interested in the details of the derivation might jump straight to Tables 1–4 for a reference of possible topological phonon systems and the example section for an illustration of these tables.

For noninteracting electrons, the ground state is given by a Slater determinant of all states below the chemical potential. The topological properties are then encoded in the projector $P(\vec{k})$ onto the filled bands. Moreover, one can simplify the discussion by introducing a "flattened Hamiltonian" $Q(\vec{k}) = 1-2P(\vec{k})$, which assumes the eigenvalues ± 1 for filled (empty) bands (53).

The topological indices are now encoded in the mappings from the Brillouin zone to an appropriate target space induced by $Q(\vec{k})$. In the absence of any symmetries the target space are the set of complex Grassmanians. In even dimensions, these mappings are characterized by Chern numbers that lie in $\mathbb{Z}$ (marked in blue in Table 1). In case that the chiral symmetry $\mathcal{S}$ is present, the $Q(\vec{k})$ matrices have additional structure. This structure can be used to block–off-diagonalize them (21, 53)

$$Q\left(\vec{k}\right) = \begin{pmatrix} 0 & q\left(\vec{k}\right) \\ q^{\dagger}\left(\vec{k}\right) & 0 \end{pmatrix}, \qquad [15]$$

and to obtain a mapping from the Brillouin zone to the space of unitary matrices. In odd dimensions, the homotopy group of these maps is described by a winding number $\in\mathbb{Z}$ (marked in red in Table 1). These two types of indices are called the primary indices.

Table 1. The 10-fold way

	Symmetries			Dimensions		
Class	$\mathcal{T}$	$\mathcal{C}$	$\mathcal{S}$	1	2	3
A	0	0	0	0	$\mathbb{Z}$	0
AIII	0	0	1	$\mathbb{Z}$	0	$\mathbb{Z}$
AI	+	0	0	0	0	0
BDI	+	+	1	$\mathbb{Z}$	0	0
D	0	+	0	$\mathbb{Z}_2$	$\mathbb{Z}$	0
DIII	−	+	1	$\mathbb{Z}_2$	$\mathbb{Z}_2$	$\mathbb{Z}$
AII	−	0	0	0	$\mathbb{Z}_2$	$\mathbb{Z}_2$
CII	−	−	1	$2\mathbb{Z}$	0	$\mathbb{Z}_2$
C	0	−	0	0	$2\mathbb{Z}$	0
CI	+	−	1	0	0	$2\mathbb{Z}$

The color code is explained in the main text. This table also applies to the high-frequency problem of nonreciprocal metamaterials. The first column gives the standard names of the symmetry groups. The next three columns serve to indicate the absence (0) or presence (1, +, –) of a given symmetry. The $+/-$ signal that the respective symmetry squares to ± 1. The last columns finally provide the information if the band structures in the given dimension is characterized by an integer number ($\mathbb{Z}$), an even integer ($2\mathbb{Z}$), or a binary index ($\mathbb{Z}_2$).

Table 2. Indices for high-frequency reciprocal metamaterials with $\Gamma = 0$

	Symmetries			Dimensions		
Class	$\mathcal{T}/\mathcal{T}^*$	$\mathcal{C}$	$\mathcal{S}$	1	2	3
BDI	+	+	1	$\mathbb{Z}$	0	0
DIII	$+/-$	+	1	$\mathbb{Z}_2$	$\mathbb{Z}_2$	0
AII	$+/-$	0	0	0	$\mathbb{Z}_2$	$\mathbb{Z}_2$
CII	$+/-$	−	1	0	0	$\mathbb{Z}_2$
CI	+	−	1	0	0	$2\mathbb{Z}$

There is always a $\mathcal{T}$ symmetry squaring to +1, which can be augmented to $\mathcal{T}^*$ squaring to −1.

Additional indices can be derived from the primary ones when more symmetries are present. By constructing families of $d-1$ - and $d-2$ -dimensional systems whose interpolation constitute a d-dimensional Hamiltonian with a primary index, one can establish topologically distinct families of such lower-dimensional band structures through descendant indices. They are marked in light blue (light red) for descendants of the Chern (winding) numbers. Moreover, certain symmetries restrict the primary indices to even values denoted by $2\mathbb{Z}$ in Table 1. Concrete formulas for the Chern and winding numbers are given in *Supporting Information*. For general formulas for the descendent indices, we refer to ref. 53 and references therein. This overview concludes our discussion of the electronic classification, which is summarized in Table 1.

For mechanical systems, a few characteristics deserve special attention. First, in a mechanical system, no Pauli principle is available to give a band as a whole a thermodynamic relevance. However, it is clear that the projector to a given number of isolated bands encodes the topological properties of the (high-frequency)[¶] gap above these bands. For engineering applications in the respective frequency range, this is good enough. Second, before we apply the topological classification of Table 1 blindly to a generic mechanical system it is beneficial to first structure the problems at hand by "nontopological" considerations.

There are two natural properties that divide the mechanical problems into four different classes: (*i*) a mechanical system can either be made from "passive" building blocks, or it can incorporate nonreciprocal elements. In our formulation, they distinguish themselves by the absence or presence of a Γ term in the Hamiltonian 4. (*ii*) The formulation of topological indices is rather different for the case where we target the gap around $\omega = 0$ (relevant for thermodynamic or ground-state properties) or a gap at finite frequencies. In the following, we discuss the different combinations of finite vs. zero frequency and reciprocal vs. nonreciprocal materials separately.

High-Frequency Nonreciprocal Metamaterials. The presence of $\Gamma \neq 0$ puts the high-frequency problem of nonreciprocal metamaterials on equal footing with the electronic problem. Therefore, no further constraints are imposed and the full Table 1 is explorable.

High-Frequency Reciprocal Metamaterials. For reciprocal high-frequency problems, one can in principle apply the classification scheme to D rather than H, as already D is a Hermitian matrix.[#] The reality of D ensures the presence of a $\mathcal{T}$ symmetry that squares to +1. One can augment this $\mathcal{T}$ symmetry to an antiunitary

[¶] "High" is to be understood as "nonzero."

[#] Remember that $\sqrt{D}$ and D share the same eigenvectors, and we continue with H to keep the discussion unified.

Table 3. Indices for low-frequency reciprocal metamaterials with $\Gamma = 0$

	Symmetries			Dimensions		
Class	$\mathcal{T}/\mathcal{T}^*$	$\mathcal{C}/\mathcal{C}^*$	$\mathcal{S}$	1	2	3
BDI	+	+	1	$\mathbb{Z}$	0	0
DIII	+/−	+	1	$\mathbb{Z}_2$	$\mathbb{Z}_2$	0
CII	+/−	+/−	1	0	0	$\mathbb{Z}_2$

Both the $\mathcal{C}$ and $\mathcal{T}$ symmetry need to be augmented to reach classes where these symmetries square to −1.

symmetry $\mathcal{T}^*$ that squares to −1 via an appropriate unitary symmetry U_{aug}:

$$U_{\mathcal{T}^*} = U_{\text{aug}} \circ U_{\mathcal{T}} \quad \text{with} \quad U_{\mathcal{T}^*}^2 = -1. \qquad [16]$$

However, it is important to note that the simultaneous presence of both a $\mathcal{T}$ and $\mathcal{T}^*$ symmetry will force certain indices to vanish. A careful but straightforward analysis (*Supporting Information*) of the indices results in Table 2 relevant for reciprocal high-frequency problems.

Low-Frequency Reciprocal Metamaterials. Topological band structures with nontrivial gaps around zero frequency are relevant for floppy modes in static problems (8) or thermodynamic properties (34) of jammed granular media. As argued above, the structure of the equations of motion imply a $\mathcal{C}$ symmetry around $\omega = 0$. In the absence of Γ, an additional $\mathcal{T}$ symmetry is present. Both this built-in symmetries canonically square to +1. As in the case of high-frequency reciprocal materials, one can augment these symmetries by unitary symmetries to reach classes where the augmented ones square to −1. Table 3 summarizes the resulting possibilities for topological indices in this setup.

Low-Frequency Nonreciprocal Metamaterials. Similarly to the high-frequency nonreciprocal metamaterials, the generic $\mathcal{T}$ symmetry is absent here. Hence, there can arise effective $\mathcal{T}$ symmetries that either square to +1 or −1 without the need to augment the generically present one to reach classes where $\mathcal{T}^2 = -1$. Given that we deal with the gap at $\omega = 0$, however, guarantees the generic $\mathcal{C}$ symmetry, which in turn can be enriched to one that squares to −1. The resulting possible topologies are shown in Table 4.

For the case of zero-frequency indices, the construction of H with the help of $\sqrt{D}$ necessary leads to trivial phases (*Supporting Information*). However, in refs. 5 and 35, it was shown how a decomposition $D = QQ^T$ allowing for nontrivial $\mathbb{Z}$ indices in class BDI can be constructed for Maxwell frames. How one can construct similar formulations for the other symmetry classes shown in Tables 3 and 4 is an interesting open problem.

Table 4. Indices for low-frequency nonreciprocal metamaterials with $\Gamma \neq 0$

	Symmetries			Dimensions		
Class	$\mathcal{T}$	$\mathcal{C}/\mathcal{C}^*$	$\mathcal{S}$	1	2	3
BDI	+	+	1	$\mathbb{Z}$	0	0
D	0	+	0	$\mathbb{Z}_2$	$\mathbb{Z}$	0
DIII	−	+	1	$\mathbb{Z}_2$	$\mathbb{Z}_2$	$\mathbb{Z}$
CII	−	+/−	1	0	0	$\mathbb{Z}_2$
C	0	+/−	0	0	$2\mathbb{Z}$	0

Here, only the $\mathcal{C}$ symmetry needs to be augmented as no generic $\mathcal{T}$ symmetry is present.

Examples

To clarify and reinforce our approach, we provide a set of examples. We directly consider discrete models. An example on how to extract a discrete description of a continuum model is provided in *Supporting Information*. The degrees of freedom are assumed to be ideal 1D or 2D pendula. The desired D matrix can be obtained by coupling the different pendula by springs. To encode negative coupling elements, or in case of geometrical obstructions, it might be required to replace a spring coupling by a more involved coupling composed of springs and deflection levers, as for example, in ref. 11. Note, that although we consider pendula as our local oscillator, all examples are generic and can be applied to any set of mechanical modes.

The last ingredient we need is a $\Gamma \neq 0$. One option is to engage the Lorentz force, which directly provides such a coupling. Another possibility is to use spinning tops, or gyroscopes as in refs. 12 and 30. We consider a symmetric gyroscope with a fixed point (different from the center of mass) about which it can rotate (Fig. 2). For our considerations, there will be no external moment along the principal axis passing through the center of mass, rendering this rotation a conserved quantity. Hence, there are only two degrees of freedom left.

In a constant gravitational field, we can use the direction of the field to define a z axis. The potential energy of the gyroscope has a minimum, and one can linearize the problem about this minimum. The resulting problem has two effective degrees of freedom, which we choose to be displacements along the x and y direction. The equation of motion for the linearized system is then of the form (*Supporting Information*)

$$\begin{pmatrix} \dot{x} \\ \dot{y} \\ \ddot{x} \\ \ddot{y} \end{pmatrix} = \begin{pmatrix} 0 & 0 & 1 & 0 \\ 0 & 0 & 0 & 1 \\ -\mu & 0 & 0 & \gamma \\ 0 & -\mu & -\gamma & 0 \end{pmatrix} \begin{pmatrix} x \\ y \\ \dot{x} \\ \dot{y} \end{pmatrix} + \begin{pmatrix} 0 \\ 0 \\ M_x \\ M_y \end{pmatrix},$$

where γ is proportional to the spinning speed of the gyroscope and $M_{x/y}$ are external moments coupling to it. Such moments arise, for example, from the couplings to neighboring degrees of freedom. For multiple gyroscopes, this allows us to obtain

$$\Gamma = \gamma \begin{pmatrix} 0 & 1 \\ -1 & 0 \end{pmatrix}. \qquad [17]$$

These are all elements we need to discuss the following examples. Although every model has a high-frequency and a low-frequency symmetry part, we are only looking at the former, where the generic particle-hole symmetry is irrelevant. For a detailed discussion of certain low-frequency models, we refer to refs. 5 and 35.

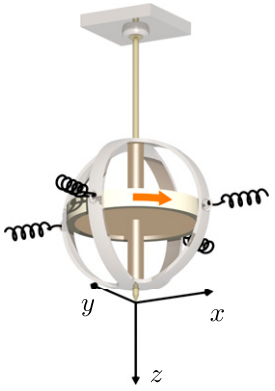

Fig. 2. Coordinate system for a spinning gyroscope.

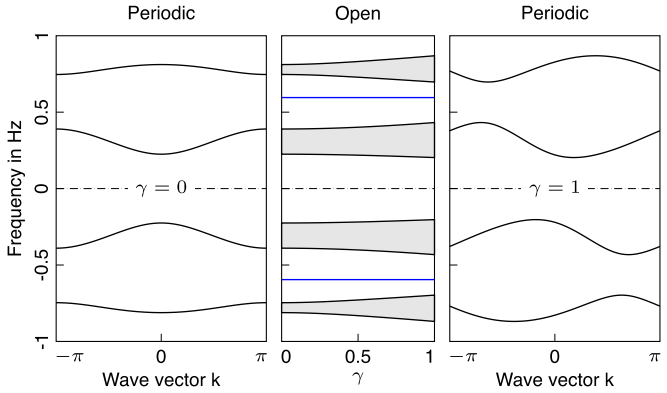

Fig. 3. Spectra of examples belonging to classes BDI ($\gamma = 0$) and AIII ($\gamma \neq 0$). (*Left*) The band structure of the BDI model given in Eq. **18**. (*Middle*) Spectrum of an open AIII chain as a function of γ. Blue lines denote edge modes, whereas the gray areas represent the bulk modes. (*Right*) The band structure of the AIII model for $\gamma = 1$. Parameters chosen to obtain the figures are: $t = 2$ Hz^2, $t' = 10$ Hz^2, and $\mu = 14$ Hz^2.

We start with the simplest possible 1D model with a nontrivial index below. After its discussion, we show how one can combine several copies of such simple building blocks to reach a number of other symmetry classes in 1D. Finally, we provide each an example of a 2D system with a nonvanishing Chern number and a model where we use the idea of symmetry enrichment.

Class BDI in 1D. Probably the simplest model available is the analog of the Su–Schrieffer–Heeger model (54). It can be realized through a chain of 1D pendula, coupled through springs with alternating spring constants t and t'. Its dynamics is governed by

$$D(k;t,t') = \begin{pmatrix} \mu & -t - t'e^{-ik} \\ -t - t'e^{ik} & \mu \end{pmatrix}, \qquad \Gamma = 0, \qquad [18]$$

and $\mu > |t| + |t'|$ for positive definiteness.

The model has a $\mathcal{S}$ symmetry (chiral symmetry), which can already be seen on the level of the D matrix:

$$U_{\mathcal{S}} D(k) + D(k) U_{\mathcal{S}} = 2\mu U_{\mathcal{S}}, \qquad U_{\mathcal{S}} = \begin{pmatrix} 1 & 0 \\ 0 & -1 \end{pmatrix}.$$

The symmetry translates into a $\mathcal{S}$ symmetry of $\pm\sqrt{D}$, which are the two blocks of $H(\vec{k})$ after block-diagonalizing it:

$$TH(k)T^\dagger = \begin{pmatrix} \sqrt{D}(k) & 0 \\ 0 & -\sqrt{D}(k) \end{pmatrix}, \quad T = \frac{1}{\sqrt{2}} \begin{pmatrix} 1 & 1 \\ 1 & -1 \end{pmatrix}. \qquad [19]$$

In addition, the model has $\mathcal{T}$ symmetry and therefore $\mathcal{C}$ symmetry as well, which puts it into symmetry class BDI. This class features a winding number through its $Q(k)$ matrix

$$Q(k) = \begin{pmatrix} 0 & q(k) \\ q^*(k) & 0 \end{pmatrix}, \qquad q(k) = c(k)\left(t + t'e^{-ik}\right), \qquad [20]$$

with $c(k) \in \mathbb{R}$. The matrix is already in block–off-diagonal form, and hence, the winding number $n \in \mathbb{Z}$ is given by (*Supporting Information*)

$$n = \frac{i}{2\pi} \int q(k)^{-1} q'(k) dk = \begin{cases} 0 & t < t' \\ -1 & t > t' \end{cases}.$$

The band structure of the periodic system is shown in Fig. 3, *Left*, and the eigenfrequencies of the open system are given in Fig. 3, *Middle*, at the point $\gamma = 0$ (see below). Up to here, we were free to discuss the problem in terms of $D(k)$ instead of $\sqrt{D}(k)$. However, this is no longer possible once $\Gamma \neq 0$, as considered in the next example.

Class AIII in 1D. The above model is now supplemented by a nonvanishing Γ matrix. This breaks the $\mathcal{T}$ and the particle-hole symmetry, but the chiral symmetries on the two subspaces (positive/negative eigenfrequencies) are left invariant. In the case that $|\gamma| \ll |t - t'|$, all spectral gaps remain open, and hence the topological index will not change. The evolution of the gap as well as of the edge mode (which stays invariant) for increasing γ is shown in Fig. 3, *Middle*. An exemplary band structure for $\gamma = 1$ can be seen in Fig. 3, *Right*.

Breaking $\mathcal{T}$ and $\mathcal{C}$ symmetry of the BDI model did not change the topological index, because the index relies on chiral symmetry only.

Class D in 1D. To break the $\mathcal{S}$ symmetry while keeping $\mathcal{C}$ symmetry, we need to add further degrees of freedom. Starting point are two copies, $D(k;t,t')$ and $D(k;s,s')$, of the above BDI model:

$$D(k;t,t',s,s') = \begin{pmatrix} D(k;t,t') & 0 \\ 0 & D(k;s,s') \end{pmatrix}. \qquad [21]$$

We assume that both share the same μ. For $\Gamma = 0$, the model belongs to BDI and the winding number of the lowest two bands is given by

$$n = \begin{cases} 0 & t < t' \text{ and } s < s' \\ 1 & (t > t' \text{ and } s < s') \text{ or } (t < t' \text{ and } s > s'). \\ 2 & t > t' \text{ and } s > s' \end{cases}$$

By choosing $t \neq s$ or $s' \neq t'$, and turning on $\Gamma \neq 0$, we break all of the symmetries except for the high-frequency $\mathcal{C}$ symmetry

$$U_{\mathcal{C}} = \begin{pmatrix} 1 & 0 & 0 & 0 \\ 0 & -1 & 0 & 0 \\ 0 & 0 & 1 & 0 \\ 0 & 0 & 0 & -1 \end{pmatrix} \kappa.$$

This puts the model into symmetry class D.

The $\mathbb{Z}$ index gets reduced to a $\mathbb{Z}_2$ index,

$$p = \begin{cases} 0 & (t - t')(s - s') > 0 \\ 1 & (t - t')(s - s') < 0 \end{cases},$$

the parity of the winding number. In the case that $p = 0$, the breaking of the $\mathcal{S}$ symmetry makes the cases $n = 0$ and $n = 2$

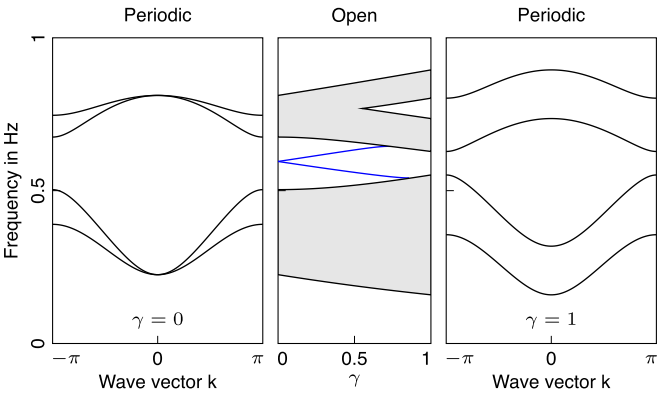

Fig. 4. Spectra of examples belonging to classes BDI ($\gamma = 0$) and D (trivial) ($\gamma \neq 0$). (*Left*) The band structure of the periodic BDI model given in Eq. **21**. (*Middle*) Spectrum of the open D model. The parity of the winding number is even; therefore, the topological edge modes are not protected upon turning on $\gamma \neq 0$. (*Right*) The band structure of the D model for $\gamma = 1$. Parameters chosen to obtain the figures are: $t = 2$ Hz^2, $t' = 10$ Hz^2, $s = 4$ Hz^2, $s' = 8$ Hz^2, and $\mu = 14$ Hz^2.

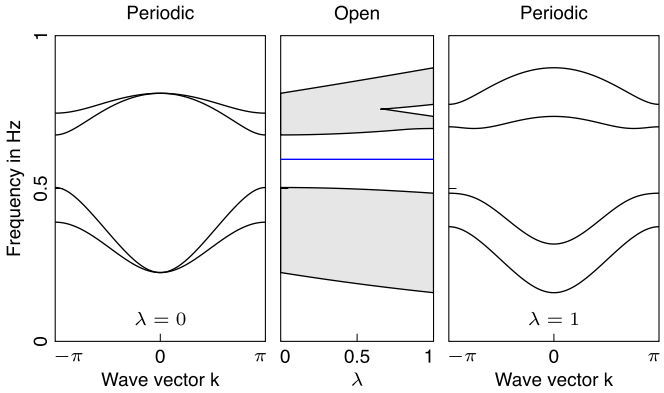

Fig. 5. Spectra of examples belonging to classes BDI ($\gamma = 0$) and D (nontrivial) ($\gamma \neq 0$). Here, the parity of the winding number is odd, and hence the topological edge mode is protected even when $\gamma \neq 0$. Parameters chosen to obtain the figures are: $t = 2$ Hz^2, $t' = 10$ Hz^2, $s = 8$ Hz^2, $s' = 4$ Hz^2, and $\mu = 14$ Hz^2.

equivalent, as the two edge modes can hybridize and disappear from the gap (Fig. 4). In the case that $p = 1$, the single-edge mode from the BDI model remains as displayed in Fig. 5.

Class A in 2D. The topology of the discussed 1D models relied on the presence of a $\mathcal{S}$ ($\mathcal{C}$) symmetry. The next model we look at does not rely on any symmetries at all, and the topological index will be the Chern number. To obtain a nonvanishing Chern number, we need to break $\mathcal{T}$ symmetry by choosing $\Gamma \neq 0$, and therefore we need to have at least two degrees of freedom per unit cell. The Γ matrix can only take the form from Eq. **17**, which leaves us with finding a suitable D matrix.

To this end, it is helpful to transform $H(\vec{k})$, as in Eq. **19**, to

$$THT^\dagger = \begin{pmatrix} \sqrt{D} + \frac{i}{2}\Gamma & -\frac{i}{2}\Gamma \\ -\frac{i}{2}\Gamma & -\sqrt{D} + \frac{i}{2}\Gamma \end{pmatrix},$$

and to define

$$\tilde{H}(k_x, k_y; \alpha) = \begin{pmatrix} \sqrt{D} + \frac{i}{2}\Gamma & -\alpha\frac{i}{2}\Gamma \\ -\alpha\frac{i}{2}\Gamma & -\sqrt{D} + \frac{i}{2}\Gamma \end{pmatrix}. \qquad [22]$$

By varying $\alpha \in [0,1]$, we can continuously deform $H(k_x, k_y)$ into a model with two decoupled blocks $\pm\sqrt{D} + \frac{i}{2}\Gamma$. If the bulk gaps remain opened during the interpolation from $\alpha = 0$ to $\alpha = 1$, the Chern number of any subspace will not change, and we can focus on constructing nontrivial subblocks of $\tilde{H}(k_x, k_y; 0)$.

We now focus on the block characterized by $\sqrt{D} + \frac{i}{2}\Gamma$. This matrix is Hermitian and can be written as

$$\sqrt{D}(k_x, k_y) + \frac{i}{2}\Gamma = \mu(k_x, k_y)1 + \vec{d}(k_x, k_y) \cdot \vec{\sigma},$$

where σ_i are the Pauli matrices

$$\sigma_1 = \begin{pmatrix} 0 & 1 \\ 1 & 0 \end{pmatrix}, \quad \sigma_2 = \begin{pmatrix} 0 & -i \\ i & 0 \end{pmatrix}, \quad \sigma_3 = \begin{pmatrix} 1 & 0 \\ 0 & -1 \end{pmatrix},$$

and $\vec{d}(k_x, k_y) \in \mathbb{R}^3$, a vector with real coefficients. The d vector contains all of the information about the eigensolutions of the problem and therefore also about the Chern numbers of the bands. In the case that $|\vec{d}(k_x, k_y)| \neq 0$ for all k_x and k_y, we can define $\vec{n}(k_x, k_y) = \vec{d}/|\vec{d}|$. Upon varying k_x and k_y through the Brillouin zone $\vec{n}$ traces out a closed surface in $\mathbb{R}^3$. It can be shown that the number of net encircling of the origin by this surface corresponds to the Chern number of the lower band (55).

A possible choice of coefficients giving rise to a nontrivial band structure is

$$\begin{aligned} d_1 &= \cos k_x, \\ d_2 &= \sin k_x + \sin k_y - \gamma, \\ d_3 &= \cos k_y. \end{aligned} \qquad [23]$$

Owing to the fact that $\sqrt{D}$ and D share the same eigenvalues, it is easy to see that the dynamical matrix is parameterized by

$$D(k_x, k_y) = \tilde{\mu}1 + t\,\vec{d}(k_x, k_y; \gamma = 0) \cdot \vec{\sigma} \qquad [24]$$

for some suitable $\tilde{\mu}$ and t.

The approximative argument at $\alpha = 0$ is supported by a numerical calculation for $\alpha = 1$, which confirms the presence of a nonzero Chern number. In addition, we show the spectrum of a semiinfinite cylinder in Fig. 6, revealing the existence of an edge mode within the bulk gap.

The presented model is a minimal model in the sense of required degrees of freedom. However, it is probably not the simplest model for an actual implementation. For such a purpose, a simpler model can be found in ref. 12.

Class AII in 2D. Up to here, all examples we looked at were based on symmetries that square to +1. However, we can also supplement symmetries to obtain new symmetries that can square to −1. As an example, we discuss the quantum spin Hall-like system presented in ref. 11. It mimics a Hofstadter model (56) at $\Phi = 1/3$ flux plus its time-reversed copy. Its dynamical matrix is

$$D(\vec{k}) = \begin{pmatrix} D_1(\vec{k}) & D_2(\vec{k}) \\ -D_2(\vec{k}) & D_1(\vec{k}) \end{pmatrix},$$

$$D_1(\vec{k}) = -\mu 1 + 2t \begin{pmatrix} 2\cos(k_y) & 1 & e^{ik_x} \\ 1 & -\cos(k_y) & 1 \\ e^{-ik_x} & 1 & -\cos(k_y) \end{pmatrix},$$

$$D_2(\vec{k}) = i2\sqrt{3}t \sin(k_y) \begin{pmatrix} 0 & 0 & 0 \\ 0 & 1 & 0 \\ 0 & 0 & -1 \end{pmatrix},$$

and $\Gamma = 0$.

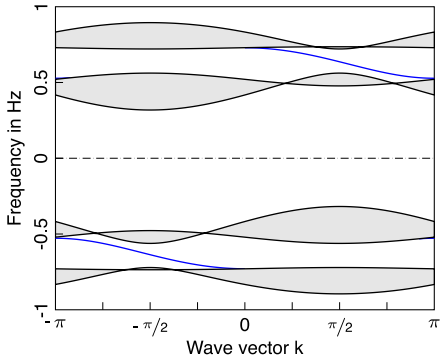

Fig. 6. Spectrum of the class A model on a semiinfinite cylinder as a function of the wave vector around the cylinder. Gray areas represent a continuum of bulk modes, whereas blue lines denote the chiral surface modes. Parameters chosen to obtain the figure are: $t = 5$ Hz^2, $\tilde{\mu} = 16$ Hz^2, and $\gamma = 1$ Hz^2.

The structure of $D(\vec{k})$ carries a $\mathcal{T}$ symmetry whose antiunitary representation is just given by the complex conjugation κ, that is, $U_{\mathcal{T}} = 1\kappa$. Therefore, this symmetry squares to 1. However, there is an additional structure, which allows to generate an augmented symmetry $\mathcal{T}^*$,

$$U_{\mathcal{T}^*} = U_{\text{aug}} \circ \kappa = \begin{pmatrix} 0 & 1 \\ -1 & 0 \end{pmatrix} \kappa, \qquad U_{\mathcal{T}^*}^2 = -1,$$

which gets lifted to a $\mathcal{T}^*$ symmetry of $H(\vec{k})$. Otherwise, there are no relevant symmetries present away from $\omega = 0$, which puts the problem into symmetry class AII. Repeating the calculation from the previous model results in Fig. 7. For further details on this model, we refer directly to ref. 11.

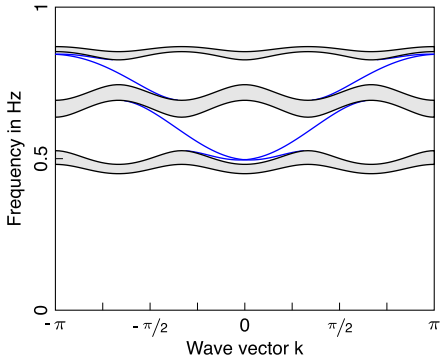

Fig. 7. Spectrum of the class AII model on a semiinfinite cylinder as a function of the wave vector around the cylinder. Parameters chosen to obtain the figure are: $t = 2$ Hz^2 and $\mu = (6 + 2\sqrt{3})t$.

Conclusions

In summary, we have developed a framework to map the equations of motion of a set of coupled linear mechanical oscillators to a quantum-mechanical tight-binding problem. Using this mapping, we showed how one can import the topological classification of noninteracting electron systems to the realm of classical mechanical metamaterials. Using the presence or absence of nonreciprocal elements as a key aspect of metamaterials, we further adapted the electronic classification to mechanical problems.

With our work, we provide the stage for the development of potentially new classes of materials, where topological boundary modes can be used to provide a specific functionality. Moreover, we help to clarify the recent literature in the field, where topological phonon modes have been predicted without an overarching framework. We hope that, with the extensive example section, we provided the reader with the tools and concepts to construct more topological phonon models using simple building blocks.

Many directions in the field of topological mechanical metamaterials are still unexplored. Obvious problems to be solved are the presentation of a topological surface mode in a 2D or 3D continuous material or the miniaturization of the effects observed at the centimeter scale down to micrometer scale. Moreover, examples of materials in many of the possible symmetry classes characterized in this report have neither been theoretically proposed nor experimentally implemented. We hope that, with this work, we stimulate research in this direction. Moreover, our results also provide the framework to import ideas based on crystalline symmetries.

Finally, the efficient characterization of model materials according to their topological properties is an important open problem. In electronic systems, the search for topological band structures is now routinely done using high-throughput ab initio calculations in combination with advanced numerical tools (57) to determine the topological indices. Our framework should provide the basis for a similar approach in mechanical metamaterials and therefore open the route to various applications based on topological boundary modes.

ACKNOWLEDGMENTS. We acknowledge fruitful discussions with O. R. Bilal, T. Bzdušek, C. Daraio, and A. Soluyanov. This work was supported by the Swiss National Science Foundation.

1. Cummer SA, Christensen J, Alù A (2016) Controlling sound with acoustic metamaterials. *Nat Rev Mater* 1(3):16001.
2. Kushwaha MS, Halevi P, Dobrzynski L, Djafari-Rouhani B (1993) Acoustic band structure of periodic elastic composites. *Phys Rev Lett* 71(13):2022–2025.
3. Liu Z, et al. (2000) Locally resonant sonic materials. *Science* 289(5485): 1734–1736.
4. Prodan E, Prodan C (2009) Topological phonon modes and their role in dynamic instability of microtubules. *Phys Rev Lett* 103(24):248101.
5. Kane CL, Lubensky TC (2013) Topological boundary modes in isostatic lattices. *Nat Phys* 10(1):39–45.
6. Chen BG, Upadhyaya N, Vitelli V (2014) Nonlinear conduction via solitons in a topological mechanical insulator. *Proc Natl Acad Sci USA* 111(36):13004–13009.
7. Chen BG, et al. (2016) Topological mechanics of origami and kirigami. *Phys Rev Lett* 116(13):135501.
8. Paulose J, Chen BG, Vitelli V (2015) Topological modes bound to dislocations in mechanical metamaterials. *Nat Phys* 11(2):153–156.
9. Paulose J, Meeussen AS, Vitelli V (2015) Selective buckling via states of self-stress in topological metamaterials. *Proc Natl Acad Sci USA* 112(25):7639–7644.
10. Xiao M, et al. (2015) Geometric phase and band inversion in periodic acoustic systems. *Nat Phys* 11(3):240–244.
11. Süsstrunk R, Huber SD (2015) PHYSICS. Observation of phononic helical edge states in a mechanical topological insulator. *Science* 349(6243):47–50.
12. Nash LM, et al. (2015) Topological mechanics of gyroscopic metamaterials. *Proc Natl Acad Sci USA* 112(47):14495–14500.
13. He C, et al. (2015) Acoustic topological insulator and robust one-way sound transport. arXiv:1512.03273.
14. Meeussen AS, Paulose J, Vitelli V (2016) Topological design of geared metamaterials. arXiv:1602.08769.
15. Hasan MZ, Kane CL (2010) Colloquium: Topological insulators. *Rev Mod Phys* 82(4): 3045.
16. Haldane FDM, Raghu S (2008) Possible realization of directional optical waveguides in photonic crystals with broken time-reversal symmetry. *Phys Rev Lett* 100(1):013904.
17. Rechtsman MC, et al. (2013) Photonic Floquet topological insulators. *Nature* 496(7444):196–200.
18. Hafezi M, Mittal S, Fan J, Migdall A, Taylor JM (2013) Imaging topological edge states in silicon photonics. *Nat Photonics* 7(12):1001–1005.
19. Cheng X, et al. (2016) Robust reconfigurable electromagnetic pathways within a photonic topological insulator. *Nat Mater* 15(5):542–548.
20. Kitaev AY (2009) Periodic table for topological insulators and superconductors. *AIP Conf Proc* 1134:22–30.
21. Ryu S, Schnyder AP, Furusaki A, Ludwig AWW (2010) Topological insulators and superconductors: Tenfold way and dimensional hierarchy. *New J Phys* 12(6):065010.
22. Schnyder AP, Ryu S, Furusaki A, Ludwig AWW (2008) Classification of topological insulators and superconductors in three spatial dimensions. *Phys Rev B* 78(19):195125.
23. Berg N, Joel K, Koolyk M, Prodan E (2011) Topological phonon modes in filamentary structures. *Phys Rev E Stat Nonlin Soft Matter Phys* 83(2 Pt 1):021913.
24. Po HC, Bahri Y, Vishwanath A (2014) Phonon analogue of topological nodal semimetals. *Phys Rev B* 93(20):205158.
25. Yang Z, et al. (2015) Topological acoustics. *Phys Rev Lett* 114(11):114301.
26. Kariyado T, Hatsugai Y (2016) Hannay angle: Yet another symmetry protected topological order parameter in classical mechanics. *J Phys Soc Jpn* 85(4):043001.
27. Kariyado T, Hatsugai Y (2015) Manipulation of dirac cones in mechanical graphene. *Sci Rep* 5:18107.
28. Yang Z, Zhang B (2016) Acoustic weyl nodes from stacking dimerized chains. arXiv: 1601.07966.
29. Vitelli V, Upadhyaya N, Chen BG (2014) Topological mechanisms as classical spinor fields. arXiv:1407.2890.
30. Wang P, Lu L, Bertoldi K (2015) Topological phononic crystals with one-way elastic edge waves. *Phys Rev Lett* 115(10):104302.
31. Peano V, Brendel C, Schmidt M, Marquardt F (2015) Topological phases of sound and light. *Phys Rev X* 5(3):031011.
32. Rocklin DZ, Chen BG, Falk M, Vitelli V, Lubensky TC (2016) Mechanical Weyl modes in topological Maxwell lattices. *Phys Rev Lett* 116(13):135503.
33. Rocklin DZ, Zhou S, Sun K, Mao X (2015) Transformable topological mechanical metamaterials. arXiv:1510.06389.
34. Sussman DM, Stenull O, Lubensky TC (2015) Topological boundary modes in jammed matter. arXiv:1512.04480.
35. Lubensky TC, Kane CL, Mao X, Souslov A, Sun K (2015) Phonons and elasticity in critically coordinated lattices. *Rep Prog Phys* 78(7):073901.

36. Pal RK, Schaeffer M, Ruzzene M (2016) Helical edge states and topological phase transitions in phononic systems using bi-layered lattices. *J Appl Phys* 119(8):084305.
37. Salerno G, Ozawa T, Price HM, Carusotto I (2016) Floquet topological system based on frequency-modulated classical coupled harmonic oscillators. *Phys Rev B* 93(8):085105.
38. Khanikaev AB, Fleury R, Mousavi SH, Alù A (2015) Topologically robust sound propagation in an angular-momentum-biased graphene-like resonator lattice. *Nat Commun* 6:8260.
39. Mousavi SH, Khanikaev AB, Wang Z (2015) Topologically protected elastic waves in phononic metamaterials. *Nat Commun* 6:8682.
40. Xiao M, Chen WJ, He WY, Chan CT (2015) Synthetic gauge flux and Weyl points in acoustic systems. *Nat Phys* 11(11):920–924.
41. Ni X, et al. (2015) Topologically protected one-way edge mode in networks of acoustic resonators with circulating air flow. *New J Phys* 17(5):053016.
42. Wang YT, Luan PG, Zhang S (2015) Coriolis force induced topological order for classical mechanical vibrations. *New J Phys* 17(7):073031.
43. Fleury R, Sounas DL, Sieck CF, Haberman MR, Alù A (2014) Sound isolation and giant linear nonreciprocity in a compact acoustic circulator. *Science* 343(6170):516–519.
44. Teo JCY, Fu L, Kane CL (2008) Surface states and topological invariants in three-dimensional topological insulators: Application to $Bi_{1-x}Sb_x$. *Phys Rev B* 78(4):045426.
45. Fu L (2011) Topological crystalline insulators. *Phys Rev Lett* 106(10):106802.
46. Hsieh TH, et al. (2012) Topological crystalline insulators in the SnTe material class. *Nat Commun* 3:982.
47. Xu SY, et al. (2012) Observation of a topological crystalline insulator phase and topological phase transition in $Pb_{1-x}Sn_xTe$. *Nat Commun* 3:1192.
48. Liu CX, Zhang RX, VanLeeuwen BK (2014) Topological nonsymmorphic crystalline insulators. *Phys Rev B* 90(8):085304.
49. Alexandradinata A, Fang C, Gilbert MJ, Bernevig BA (2014) Spin-orbit-free topological insulators without time-reversal symmetry. *Phys Rev Lett* 113(11):116403.
50. Alexandradinata A, Bernevig BA (2015) Spin-orbit-free topological insulators. *Phys Scr T* 164:014013.
51. Floquet G (1883) Sur les équations différentielles linéaires à coefficients périodiques. *Ann l'Écol Norm Sup* 12:47–88.
52. Lindner NH, Refael G, Galitski V (2011) Floquet topological insulator in semiconductor quantum wells. *Nat Phys* 7(6):490–495.
53. Chiu CK, Teo JCY, Schnyder AP, Ryu S (2015) Classification of topological quantum matter with symmetries. arXiv:1505.03535.
54. Su WP, Schrieffer JR, Heeger AJ (1979) Solitons in polyacetylene. *Phys Rev Lett* 42(25):1698–1701.
55. Bernevig BA, Hughes TL (2013) *Topological Insulators and Superconductors* (Princeton Univ Press, Princeton).
56. Hofstadter DR (1976) Energy levels and wave functions of bloch electrons in rational and irrational magnetic fields. *Phys Rev B* 14(6):2239.
57. Gresch D, et al. (2016) Z2Pack. Available at z2pack.ethz.ch. Accessed April 3, 2016.